Katsuhiko Funai,[1,2] Irfan J. Lodhi,[1] Larry D. Spears,[1] Li Yin,[1] Haowei Song,[1] Samuel Klein,[3] and Clay F. Semenkovich[1,4]

Skeletal Muscle Phospholipid Metabolism Regulates Insulin Sensitivity and Contractile Function

Diabetes 2016;65:358–370 | DOI: 10.2337/db15-0659

Skeletal muscle insulin resistance is an early defect in the development of type 2 diabetes. Lipid overload induces insulin resistance in muscle and alters the composition of the sarcoplasmic reticulum (SR). To test the hypothesis that skeletal muscle phospholipid metabolism regulates systemic glucose metabolism, we perturbed choline/ethanolamine phosphotransferase 1 (CEPT1), the terminal enzyme in the Kennedy pathway of phospholipid synthesis. In C2C12 cells, CEPT1 knockdown altered SR phospholipid composition and calcium flux. In mice, diet-induced obesity, which decreases insulin sensitivity, increased muscle CEPT1 expression. In high-fat diet–fed mice with skeletal muscle–specific knockout of CEPT1, systemic and muscle-based approaches demonstrated increased muscle insulin sensitivity. In CEPT1-deficient muscles, an altered SR phospholipid milieu decreased sarco/endoplasmic reticulum Ca^{2+} ATPase–dependent calcium uptake, activating calcium-signaling pathways known to improve insulin sensitivity. Altered muscle SR calcium handling also rendered these mice exercise intolerant. In obese humans, surgery-induced weight loss increased insulin sensitivity and decreased skeletal muscle CEPT1 protein. In obese humans spanning a spectrum of metabolic health, muscle CEPT1 mRNA was inversely correlated with insulin sensitivity. These results suggest that high-fat feeding and obesity induce CEPT1, which remodels the SR to preserve contractile function at the expense of insulin sensitivity.

Despite the dozens of disorders exacerbated or induced by physical inactivity (1), a sedentary lifestyle has displaced the biologically normal exercise-trained condition in industrialized countries (2). Skeletal muscle contractile function is intrinsically linked to exercise, and exercise deficiency has contributed to the emergence of obesity, type 2 diabetes, and associated comorbidities as threats to public health. These conditions are associated with systemic insulin resistance (3). Skeletal muscle is a major contributor to insulin-stimulated glucose disposal (4).

We recently reported an unexpected role for skeletal muscle lipogenesis in the pathogenesis of insulin resistance (5). Fatty acid synthase (FAS), the enzyme catalyzing the committed step in de novo lipogenesis, is suppressed in most tissues by a high-fat, high-calorie diet (6), but the opposite occurs in skeletal muscle. In mice, high-fat, high-calorie feeding increases skeletal muscle FAS activity, while muscle-specific deficiency of FAS protects mice from diet-induced muscle insulin resistance (5). The mechanism responsible for this relationship involves FAS-facilitated synthesis of phosphatidylethanolamine (PE) at the sarcoplasmic reticulum (SR) to maintain sarco/endoplasmic Ca^{2+} ATPase (SERCA) activity (7,8). In the absence of FAS, altered PE content decreased SERCA activity, increased cytosolic calcium, and triggered calcium- and AMPK-dependent pathways that increase muscle insulin sensitivity (9). Decreased SERCA activity also induced muscle weakness, consistent with previous studies (10,11).

[1]Division of Endocrinology, Metabolism and Lipid Research, Washington University in St. Louis School of Medicine, St. Louis, MO
[2]Departments of Kinesiology and Physiology, East Carolina University, Greenville, NC
[3]Division of Geriatrics and Nutritional Science, Washington University in St. Louis School of Medicine, St. Louis, MO
[4]Department of Cell Biology and Physiology, Washington University in St. Louis School of Medicine, St. Louis, MO

Corresponding author: Clay F. Semenkovich, csemenko@dom.wustl.edu.

Received 18 May 2015 and accepted 19 October 2015.

This article contains Supplementary Data online at http://diabetes.diabetesjournals.org/lookup/suppl/doi:10.2337/db15-0659/-/DC1.

K.F. and I.J.L. contributed equally to this study.

Most PE synthesis in the mammalian SR/ER is mediated by choline/ethanolamine phosphotransferase 1 (CEPT1), the terminal enzyme in the Kennedy pathway of phospholipid synthesis (12) that generates both PE and phosphatidylcholine (PC). Since FAS has been linked to changes in PE content, SR function, and insulin sensitivity, we evaluated the potential role of skeletal muscle CEPT1 in glucose metabolism. Specifically, we perturbed CEPT1 in muscle, which included the generation of a novel mouse model of muscle-specific CEPT1 deficiency, to test the hypothesis that skeletal muscle phospholipid metabolism regulates glucose metabolism.

RESEARCH DESIGN AND METHODS

Animals

The local Animal Studies Committee approved protocols. C57BL/6 ES cells were targeted with a vector (European Conditional Mouse Mutagenesis Program) carrying loxP sites flanking exon 3 of mouse *Cept1*. A karyotypically normal clone (of 10 correctly targeted) was injected into B6(Cg)-Tyrc-2J/J blastocysts and chimeric mice were bred with B6(Cg)-Tyrc-2J/J females, and then offspring were crossed with Flp recombinase transgenics to remove the neo cassette and yield floxed heterozygous *Cept1* mice (*Cept1* lox$^+$/wt). Breeding with human α-skeletal actin (HSA)-Cre mice (13) generated CEPT1 muscle-specific knockout (CEPT1-MKO) mice, which were born in expected Mendelian fashion, indistinguishable from their control littermates and fertile. Floxed mice without Cre were used as controls, since previous studies showed no phenotype in Cre-only mice. Diets were Purina 4043 control chow or Harlan Teklad TD 88137 high-fat diet (HFD).

Lentivirus-Mediated Knockdown

Plasmids encoding short hairpin (sh)RNA for mouse *Cept1* (TRCN0000103317) and *Chpt1* (TRCN0000103294) were from Open Biosystems. Packaging vector psPAX2 (identification no. 12260), envelope vector pMD2.G (no. 12259), and scrambled shRNA plasmid (no. 1864) were from Addgene. 293T cells in 10-cm dishes were transfected using Lipofectamine 2000 (Invitrogen) with 2.66 μg psPAX2, 0.75 μg pMD2.G, and 3 μg shRNA plasmid. After 48 h, media were collected, filtered using 0.45-μm syringe filters, and used to treat undifferentiated C2C12 cells. After 36 h, target cells were selected with puromycin, and then after 48 h cells were differentiated.

Metabolic Phenotyping

Chemistries were analyzed as previously described in mice fasted for 6 h (5). Leptin (Crystal Chem), adiponectin (B-Bridge International), and insulin (PerkinElmer) ELISAs were performed according to manufacturers' instructions. Glucose and insulin tolerance tests (5) were separated by a week. Body composition was determined with an EchoMRI 3-in-1 instrument (Echo Medical Systems). Free water mass was <0.1 g for all animals and did not differ by genotype. Indirect calorimetry (Oxymax; Columbus Instruments) was performed as described (5) over 24 h after acclimating mice. Cold tolerance testing was performed by fasting mice for 4 h and then placing animals in a 4°C room for 6 h. Body temperatures were determined at regular intervals with a rectal thermometer (Thermo Fisher).

Muscle Function Studies

Mouse forelimb strength was determined using a Rodent Grip Strength Meter (Harvard Apparatus), which records peak force at the time grip is lost. Ten measurements separated by 10-min rest periods were recorded, two high and two low extremes were discarded, and the remaining six values were averaged.

For treadmill running, a high-intensity protocol was used as previously described (14). Fed mice ran 1-min intervals (with 2-min rest periods) beginning at 10 m/min and increasing by 5 m/min at each interval until exhaustion (5 s at electric grid).

Whole-Body and Muscle-Specific Glucose Metabolism

Hyperinsulinemic-euglycemic clamps were performed as previously described (5). For the basal phase, blood samples were obtained, 3-[^{3}H]D-glucose was infused (0.05 μCi/min), and then 1 h later a second basal blood sample was obtained to estimate R_a or R_d (R_a = R_d for the basal phase). For the clamp phase, infusion of 3-[^{3}H]D-glucose was replaced with a solution that contained 3-[^{3}H]D-glucose (0.05 μCi/min) and regular human insulin at 2.5 mU/kg/min (with 50 mU/kg prime); D-glucose was infused to maintain blood glucose at 120 mg/dL. After 75 min of steady-state blood glucose at 120 mg/dL, a final blood sample was taken to estimate R_a and R_d during the clamp phase ($R_a \neq R_d$ for the clamp phase). Insulin-stimulated glucose disposal rate (IS-GDR) was calculated as (R_d clamp − R_d basal). Hepatic glucose production (HGP) suppression was calculated as follows: ([R_a basal − R_a clamp]/R_a basal).

2-Deoxyglucose (2DG) uptake in isolated muscles (15) was performed in paired soleus muscles with one muscle incubated with 100 μU/mL regular insulin and the other without insulin (basal). Muscles were incubated in Krebs-Henseleit buffer (KHB) plus 0.1% BSA plus 2 mmol/L sodium pyruvate plus 6 mmol/L mannitol for 15 min and then transferred to a second vial with KHB plus 0.1% BSA plus 1 mmol/L 2DG (containing 2-deoxy-[^{3}H] glucose, 6 mCi/mmol) plus 9 mmol/L mannitol (containing [^{14}C]mannitol, 0.053 mCi/mmol) for 15 min. Samples were then processed, frozen, and homogenized, and 2DG uptake was determined.

SERCA-Dependent Calcium Uptake

SR fractions isolated by differential centrifugation (5) from C2C12 myocytes or skeletal muscles were assayed as described (5,16). The reaction was initiated with SR fractions containing 150 μg protein, stopped with 0.15 mol/L KCl/1 mmol/L $LaCl_3$, and counted after collection on a membrane. SERCA-independent calcium transport was determined by assays in the presence of 10 μmol/L thapsigargin.

Phospholipid Assays

Samples reconstituted in ddH2O were mixed with extraction buffer (2:2 [vol/vol] chloroform/methanol) in the presence of internal standards: 14:0/14:0-PC (m/z 684.5 $[M+L]^+$) or 14:0/14:0-PE (m/z 634.5 $[M-H]^-$). The organic phase was collected, concentrated to dryness under nitrogen, and reconstituted in methanol. An aliquot was removed, diluted with methanol containing 0.6% LiCl, and analyzed by direct injection electrospray ionization mass spectrometry on a Thermo Vantage triple-quadruple mass spectrometer in positive mode for the analysis of PC (neutral loss of 183) species. Another aliquot was analyzed in negative mode for PE species. Intensities of individual species were compared with internal standards, and results were generated using a standard curve.

PCR and Western Blotting

Genotyping and mouse/human RT-PCR primers were based on sequences in public databases. For blotting, membranes were incubated with the following primary antibodies: anti-CEPT1 (sc-133421), anti–calmodulin-dependent kinase I (CaMKI) (sc-33165), and anti–phospho-CaMKI^{Thr177} (sc-28438) from Santa Cruz Biotechnology; anti-CaMKII (no. 3362), anti–phospho-CaMKII^{Thr286} (no. 3361), anti-AMPKα (no. 2532), anti–phospho-AMPKα^{Thr172} (no. 2531), anti-Akt (no. 9272), anti–phospho-Akt^{Thr308} (no. 9275), anti-AS160 (no. 2447), and anti–phospho-AS160^{Thr642} (no. 4228) from Cell Signaling Technology; anti-actin (A2066) from Sigma-Aldrich; and anti-OXPHOS cocktail (ab110413) from Abcam. Bands were quantified by densitometry.

Muscle Analyses

Fatty acid oxidation was assayed by incubating labeled palmitate with cell or tissue homogenates and quantifying the generation of labeled CO_2 using NaOH-containing filter paper (17). ATP content in extensor digitorum longus (EDL) muscles was measured using a kit from Abcam (ab83355). Diacylglycerol (DAG) was quantified using a Thermo Scientific LTQ Orbitrap Velos mass spectrometer after extraction essentially, as previously described (18). For electron microscopy, EDL muscles from fasted mice were fixed in modified Karnovsky fixative; postfixed in buffered osmium tetroxide; stained with uranyl acetate; embedded, sectioned, and poststained with Venable lead citrate; and imaged with a JEOL 1299EX electron microscope.

Human Studies

Fifty-five obese subjects participated in this study, which was approved by the local Human Research Protection Office. Written informed consent was obtained from all subjects before their participation. These subjects represent a subset of subjects reported previously as part of other studies (surgical intervention registration: NCT00981500) that obtained muscle tissue samples by percutaneous biopsy and evaluated skeletal muscle insulin sensitivity by using the hyperinsulinemic-euglycemic clamp procedure in conjunction with stable isotopically labeled glucose tracer, as previously described (19–21). No subject had diabetes or other serious illnesses, none used tobacco, and none were taking medications that impact lipid metabolism.

Statistics

Results are expressed as means ± SEM or means with 95% CIs. Comparisons were performed using an unpaired two-tailed Student *t* test (for two-group analyses) or two-way ANOVA with Student-Newman-Keuls post hoc test (for two by two comparisons).

RESULTS

CEPT1 Knockdown in C2C12 Cells

Skeletal muscle FAS deficiency increases insulin sensitivity in mice by activating calcium-dependent signals through the alteration of SR phospholipid composition and SERCA activity (5). These mechanisms were defined in part by studying C2C12 cells, a skeletal muscle–like cell line that models some canonical signaling pathways in mammalian muscle. To determine whether CEPT1, a critical enzyme in phospholipid synthesis, represents a lipid signaling node downstream of FAS, we knocked down CEPT1 in C2C12 cells. Lentivirus-mediated knockdown of CEPT1 (Fig. 1*A*), reported to reside in the ER/SR (12,22), decreased SR PE content compared with cells treated with a scrambled virus (Fig. 1*B* and *C*). CEPT1 knockdown also resulted in an increase in PC (Fig. 1*D* and *E*), which nearly doubled the SR PC-to-PE ratio (Fig. 1*F*). Mirroring findings with FAS inactivation and reports from others indicating that an increased PC-to-PE ratio decreases SERCA activity (5,7,8), these changes in SR phospholipids and PC-to-PE ratio resulted in decreased SERCA-dependent calcium uptake (Fig. 1*G*) and activation of the calcium signaling proteins CaMKI and CaMKII (Fig. 1*H* and *I*). Similar to FAS deficiency, CEPT1 deficiency in C2C12 cells did not alter Akt phosphorylation but increased phosphorylation of AMPK and AS160, leading to increased phosphorylated AS160 in response to insulin signaling (Fig. 1*J* and *K*). Knockdown of CEPT1 in C2C12 cells did not affect fatty acid oxidation (0.64 ± 0.04 nmol palmitate/mg/h in scrambled vs. 0.58 ± 0.03 in CEPT1 KD, $P = 0.28$). Knockdown of choline phosphotransferase-1 (ChPT1), a PC-synthesizing enzyme that resides in the Golgi (12), did not affect phospholipids, SERCA activity, or calcium signaling (Supplementary Fig. 1*A*–*I*).

Effects of HFD on CEPT1 in Mouse Skeletal Muscle

A tissue survey for CEPT1 protein by Western blotting in wild-type C57BL/6 mice showed high expression in liver, soleus muscle, heart, and brown adipose tissue (Fig. 2*A*). Western blotting of eight different muscles with different physiological characteristics and different fiber-type composition showed higher expression of CEPT1 in soleus and diaphragm (Fig. 2*B*). Both have a predominance of slow-twitch fibers, which have been linked to diet-induced insulin resistance (23,24). Six weeks of HFD feeding, which causes insulin resistance, to C57BL/6 mice increased levels of CEPT1 protein and mRNA (Fig. 2*C* and *D*), but not ChPT1 mRNA (Fig. 2*E*), in soleus muscle. Since HFD

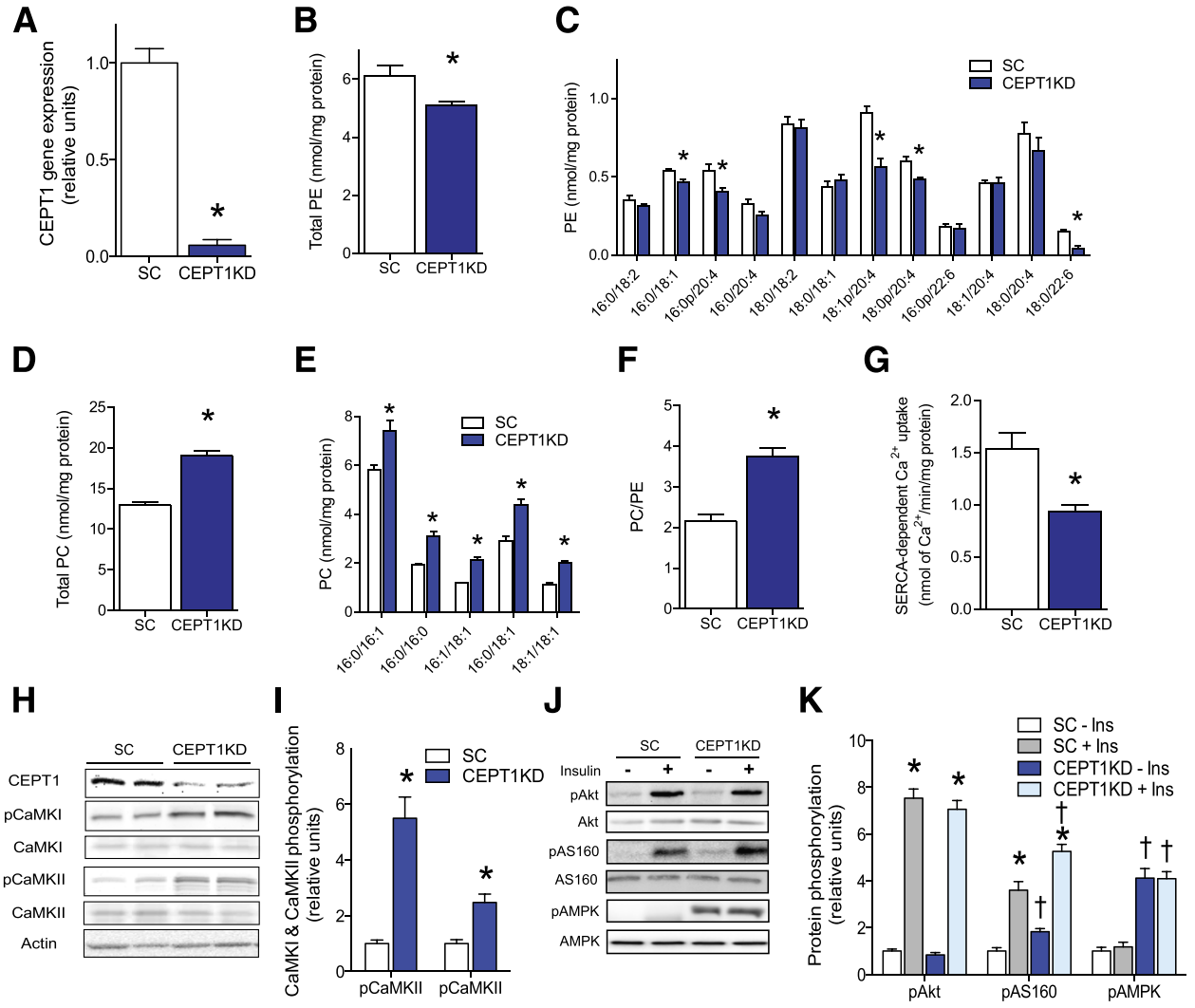

Figure 1—CEPT1 knockdown increases SR PC-to-PE ratio, calcium signaling, and insulin action in C2C12 cells. *A*: CEPT1 gene expression in C2C12 cells treated with scrambled (SC) (the control) or CEPT1 knockdown (CEPT1KD) shRNA. *B–F*: SR phospholipid composition for SC and CEPT1KD C2C12 cells. *B*: Total SR PE. *C*: SR PE species. *D*: Total SR PC. *E*: SR PC species. *F*: SR PC-to-PE ratio. *G*: SERCA-dependent calcium uptake in SC and CEPT1KD C2C12 cells. *H–K*: Western blots and quantification of proteins for SC and CEPT1KD C2C12 cells. n = 4–6/experimental condition. Data are means ± SEM. *$P < 0.05$. †$P < 0.05$ vs. SC. Ins, insulin; p, phosphorylated.

feeding in mice is known to alter PC and PE abundance in skeletal muscle (5,25), we fed mice standard chow or HFD and isolated the SR from gastrocnemius muscles. HFD caused proportional increases in both PE (Fig. 2*F* and *G*) and PC (Fig. 2*H* and *I*) in SR. There was no difference in the SR PC-to-PE ratio (a determinant of SERCA activity) or SERCA activity between chow- and HFD-fed mice (Fig. 2*J* and *K*). These data suggest that in wild-type mice, an HFD induces CEPT1 expression and increases PC and PE abundance in skeletal muscle SR, with maintenance of SR calcium handling likely due to maintenance of the SR PC-to-PE ratio.

Skeletal Muscle–Specific CEPT1 Deficiency in Mice

To determine directly whether CEPT1 deficiency improves insulin sensitivity after HFD feeding, we generated CEPT1-MKO mice. HSA-Cre, specific for skeletal muscle, was used to target the floxed CEPT1 locus (Fig. 2*L* and *M*). CEPT1-MKO mice showed proportional decreases in CEPT1 message and protein in both soleus and EDL muscles (Fig. 2*N–P*). With chow feeding, CEPT1-MKO and control mice did not differ in body weight, body composition, oxygen consumption (VO_2), respiratory quotient, glucose tolerance test, insulin tolerance test, circulating metabolites, or major metabolic hormones (Supplementary Fig. 2 and Table 1). Like CEPT1-MKO mice, skeletal muscle–specific FAS knockout mice also have no metabolic phenotype with chow feeding (5).

CEPT1-MKO and control mice were challenged with an HFD. After 6 weeks, body weight (Fig. 3*A*), body composition (Fig. 3*B*), circulating metabolites, hormones, tissue weights (Table 1), and VO_2 (Fig. 3*C*) did not differ between genotypes. However, respiratory quotient during dark cycles was increased in CEPT1-MKO compared with control mice

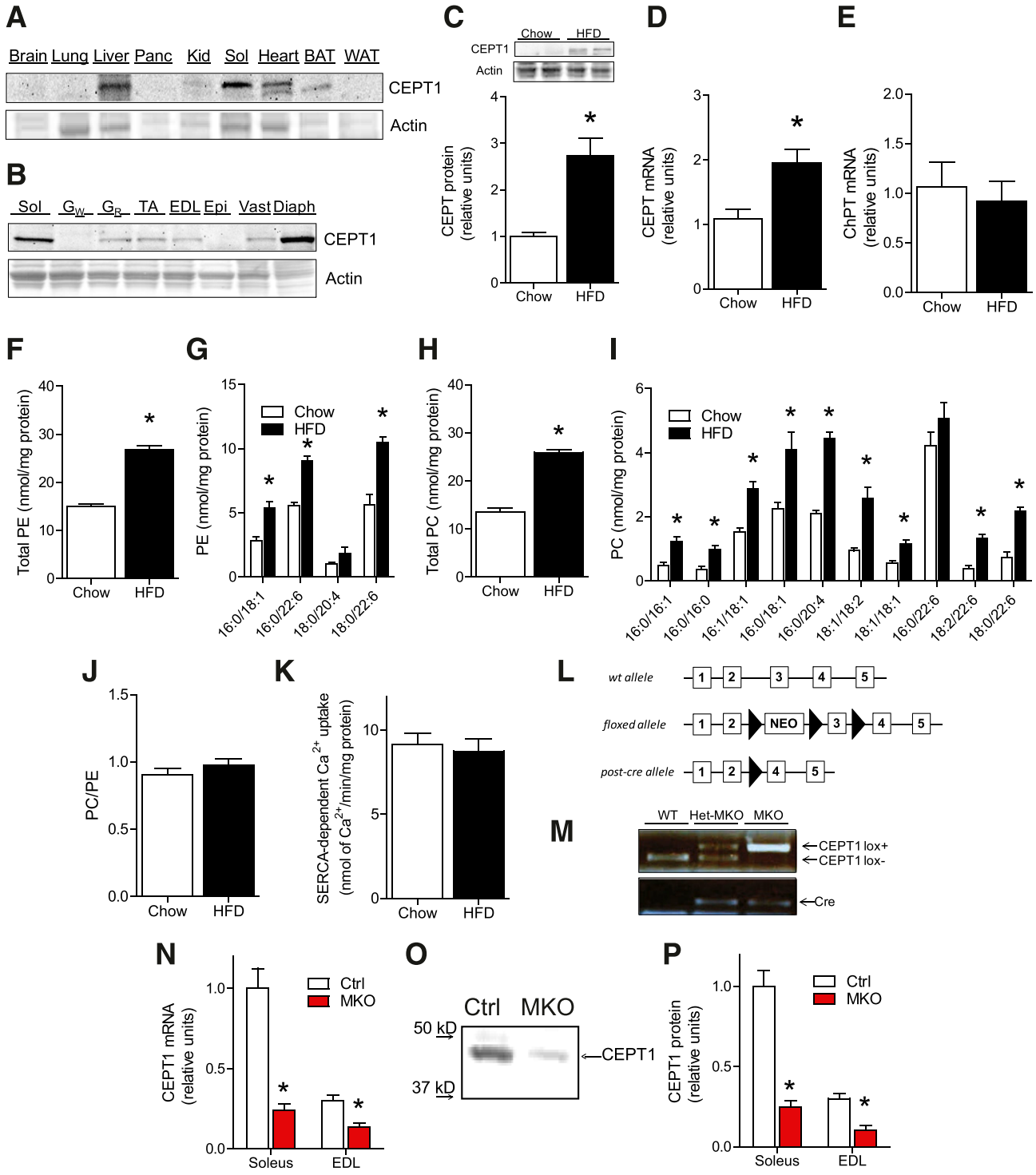

Figure 2—HFD increases mouse muscle CEPT1 but does not alter SR PC-to-PE ratio or SERCA activity, and the generation of CEPT1-MKO mice is shown. *A*: CEPT1 protein content in multiple tissues. *B*: CEPT1 protein content in multiple muscles. *C–K*: CEPT1 expression, muscle SR phospholipids, and SERCA activity in chow-fed and HFD-fed C57BL/6 mice. n = 5–8/experimental group. *C*: CEPT1 protein abundance in soleus. *D*: CEPT1 mRNA abundance in soleus. *E*: ChPT1 mRNA abundance in soleus. *F–J*: Phospholipid analyses in gastrocnemius muscles. *F*: Total SR PE. *G*: SR PE species. *H*: Total SR PC. *I*: SR PC species. *J*: SR PC-to-PE ratio. *K*: SERCA-dependent calcium uptake. *L*: Strategy yielding CEPT1-MKO mice. *M*: Genotyping PCR for wild-type (WT), heterozygous knockout in muscle (Het-MKO), and homozygous muscle knockout (MKO) mice. *N*: CEPT1 mRNA expression in soleus and EDL muscles, n = 6/experimental group. *O*: Western blot of CEPT1 in Ctrl (CEPT1 lox/lox without Cre) and homozygous muscle knockout (MKO) soleus muscles. *P*: CEPT1 protein abundance in soleus and EDL muscles, n = 6/experimental group. BAT, brown adipose tissue; Ctrl, control; Diaph, diaphragm; Epi, epitrochlearis; G_R, red gastrocnemius; G_W, white gastrocnemius; Kid, kidney; Panc, pancreas; Sol, soleus; TA, tibialis anterior; Vast, vastus lateralis. Data are means ± SEM. *$P < 0.05$.

Table 1—Chow diet–fed and HFD-fed control and CEPT1-MKO mice

	Chow		HFD	
	Control	MKO	Control	MKO
Glucose (mg/dL)	123.7 ± 5.3	131.7 ± 8.9	205.4 ± 12.5*	204.8 ± 10.5*
Free fatty acids (mmol/L)	0.434 ± 0.048	0.394 ± 0.047	0.556 ± 0.043*	0.565 ± 0.036*
Triglycerides (mg/dL)	35.92 ± 3.66	37.32 ± 1.92	54.81 ± 3.09*	53.64 ± 2.41*
Cholesterol (mg/dL)	58.5 ± 9.8	52.1 ± 6.1	162.4 ± 12.1*	155.2 ± 15.8*
Insulin (μU/mL)	4.6 ± 0.9	5.0 ± 1.7	11.8 ± 1.8*	12.3 ± 1.9*
Leptin (ng/mL)	1.4 ± 0.6	1.1 ± 0.5	5.8 ± 1.1*	6.3 ± 1.4*
Adiponectin (μg/mL)	27.5 ± 2.4	28.2 ± 3.6	25.7 ± 3.9	25.1 ± 4.1
Soleus weight (mg)	10.25 ± 0.44	10.65 ± 0.53	11.13 ± 0.69	11.36 ± 0.49
EDL weight (mg)	11.92 ± 0.63	12.13 ± 0.57	12.33 ± 0.53	12.22 ± 0.62
Liver weight (g)	0.568 ± 0.035	0.577 ± 0.041	1.182 ± 0.061*	1.128 ± 0.066*
Epididymal fat weight (g)	0.468 ± 0.048	0.492 ± 0.033	1.313 ± 0.055*	1.293 ± 0.071*

Data are means ± SEM. N = 6–12/experimental group. *By two-way ANOVA, there is a main effect ($P \leq 0.0035$) of HFD on all variables except adiponectin, soleus weight, and EDL weight.

(Fig. 3*D*), suggesting increased use of glucose by CEPT1-MKO mice when these nocturnal animals are eating.

CEPT1-MKO Mice Are Protected From Diet-Induced Insulin Resistance

Glucose and insulin tolerance testing showed that HFD-fed mice with skeletal muscle CEPT1 deficiency had improved glucose tolerance (Fig. 3*E*) and lower blood glucose after insulin administration (Fig. 3*F*) compared with controls. For clarification of site-specific effects on insulin sensitivity, hyperinsulinemic-euglycemic clamp studies were conducted in HFD-fed CEPT1-MKO and control mice (Fig. 3*G*–*J*). Consistent with glucose tolerance test and insulin tolerance test results in these animals, the glucose infusion rate, an indicator of whole-body insulin sensitivity, was twofold greater in CEPT1-MKO compared with control mice (Fig. 3*G*). The IS-GDR, an indicator of peripheral insulin sensitivity, was also twofold greater in CEPT1-MKO compared with control mice (Fig. 3*I*). There was no genotype-specific effect on insulin suppression of endogenous (mostly hepatic) glucose production (HGP suppression) (Fig. 3*J*).

Enhanced insulin sensitivity occurred without effects on adiposity (Fig. 3*B*); serum FFA, adiponectin, or leptin concentrations (Table 1); or metabolic rate (Fig. 3*C*), suggesting that muscle CEPT1 deficiency increased insulin sensitivity through effects intrinsic to muscle. To address directly the potential role of muscle in the phenotype, soleus muscles isolated from HFD-fed CEPT1-MKO and control mice were incubated in the presence of 2DG with or without 100 μU/mL insulin. Insulin-stimulated 2DG uptake in CEPT1-MKO muscle was greater than in control muscle (Fig. 3*K* and *L*). Western blotting showed that CaMKI and AMPK were activated in CEPT1-MKO muscle compared with control muscle, but there was no genotype-specific effect on Akt (Fig. 3*M* and *N*). AMPK activation would be expected to increase phosphorylation of acetyl-CoA carboxylase and AS160, both seen in CEPT1-MKO muscles (Fig. 3*M* and *N*), effects associated with increased insulin sensitivity. This same pattern of calcium-activated signaling with no effect on Akt was also seen in muscle-specific FAS knockout mice (5), suggesting that FAS and CEPT1 regulate muscle insulin sensitivity through similar mechanisms.

Muscle CEPT1 Deficiency Is Associated With Altered SR Phospholipid Composition, Disrupted Calcium Handling, and Weakness

FAS deficiency in C2C12 cells as well as in skeletal muscle alters the SR PC-to-PE ratio to decrease SERCA activity (5), and CEPT1 deficiency in C2C12 cells similarly increases SR PC:PE and decreases SERCA activity (Fig. 1), so we characterized SR phospholipids and SERCA activity in gastrocnemius muscle of MKO mice. Muscle CEPT1 deficiency in HFD-fed mice reduced SR PE (Fig. 4*A* and *B*), and increased several SR PC species (Fig. 4*C* and *D*), which increased the SR PC-to-PE ratio (Fig. 4*E*). This membrane composition change reduced SERCA-dependent calcium uptake in CEPT1-deficient muscles (Fig. 4*F*).

Intact SR calcium handling is required for normal muscle strength (26). Mimicking the effects in HFD-fed mice with skeletal muscle FAS deficiency (5), HFD CEPT1-MKO mice had decreased performance compared with control mice during high-intensity exercise tests (Fig. 4*G* and *H*) and had weaker forelimb grip strength than control mice (Fig. 4*I* and *J*). Altered SERCA activity in muscle has been reported to affect thermogenesis (27), but there was no body temperature difference between HFD-fed MKO and control mice in cold tolerance tests (Fig. 4*K*).

CEPT1, DAG, and Mitochondria

FAS deficiency does not appear to alter mitochondrial function in skeletal muscle (5), but mice with deletion of CTP–phosphoethanolamine cytidylyltransferase (ECT), the ethanolamine-specific enzyme directly upstream of CEPT1 in the Kennedy pathway, have a profound mitochondrial phenotype and increased DAG content (28).

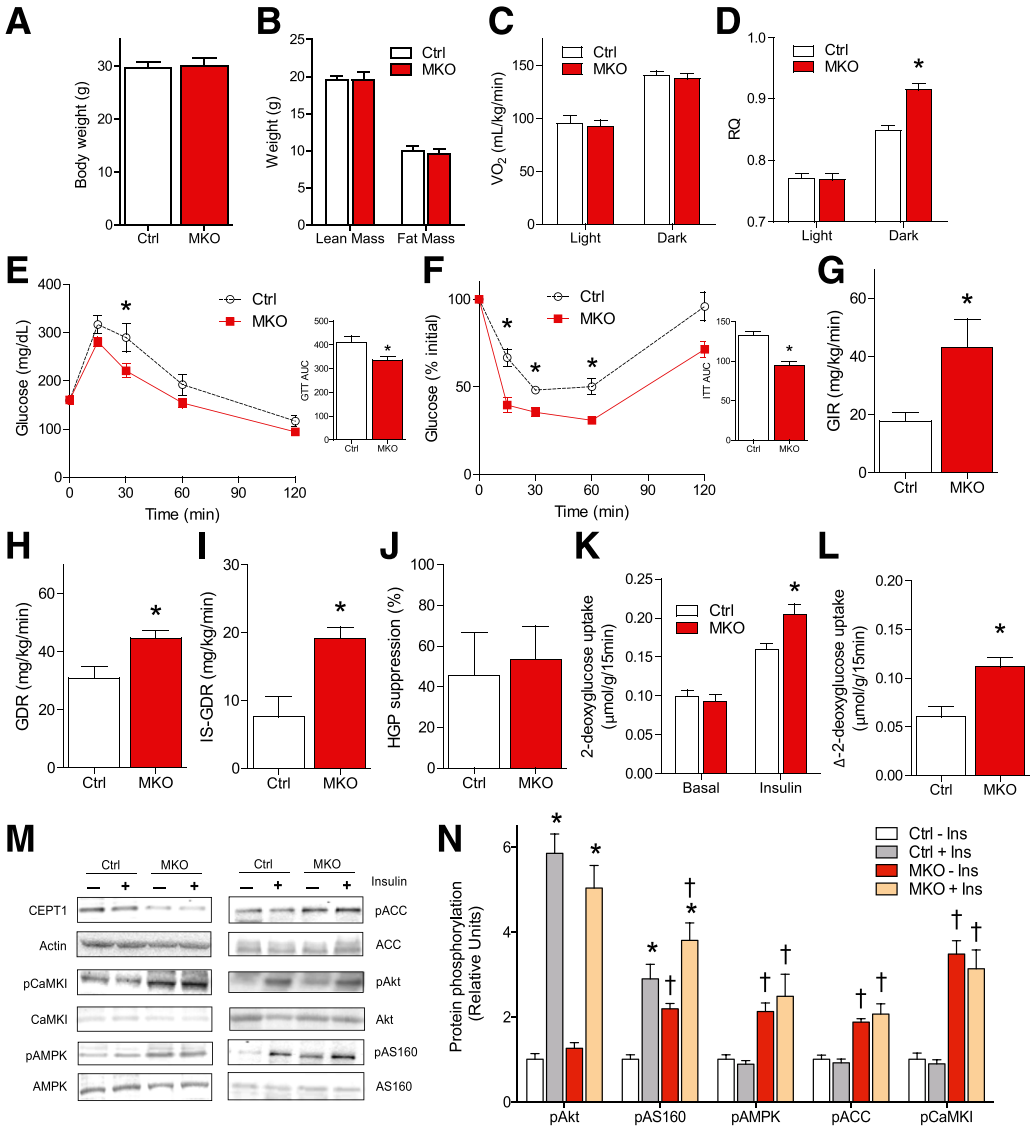

Figure 3—HFD-fed CEPT1-MKO mice are protected from diet-induced skeletal muscle insulin resistance. *A*: Body weight. *n* = 7/experimental group. *B*: Body composition by MRI. *n* = 9/experimental group. *C*: Oxygen consumption. *n* = 5/experimental group. *D*: Respiratory quotient. *n* = 5–6/experimental group. *E*: Glucose tolerance testing (GTT). Area under the curve (AUC) quantification is provided as an insert. *n* = 10/experimental group. *F*: Insulin tolerance testing (ITT). Area under the curve quantification is provided as an insert. *n* = 6–7/experimental group. *G*–*J*: Hyperinsulinemic-euglycemic clamp studies. *n* = 4/experimental group. *G*: Glucose infusion rate (GIR). *H*: Glucose disposal rate (GDR). *I*: IS-GDR. *J*: HGP suppression. *K*–*N*: Studies of isolated soleus muscles. *n* = 6/experimental group. *K*: 2DG uptake in basal and insulin-stimulated soleus. *L*: Δ2DG uptake was calculated by subtracting values of 2DG uptake in basal muscles from values of 2DG uptake in insulin-stimulated muscles. *M* and *N*: Western blot quantification of incubated soleus muscles under basal or insulin-stimulated conditions. Data are means ± SEM. **P* < 0.05. †*P* < 0.05 vs. control (Ctrl). ACC, acetyl-CoA carboxylase; Ins, insulin; p, phosphorylated; RQ, respiratory quotient.

Protein content of mitochondrial respiration complex I-V (Fig. 5*A* and *B*), gene expression of mitochondrial biogenesis markers (Fig. 5*C*), and levels of fatty acid oxidation (Fig. 5*D*) did not differ between gastrocnemius muscles from HFD-fed control and CEPT1-MKO mice. DAG content (Fig. 5*E* and *F*), ATP content (Fig. 5*G*), and apparent mitochondrial density as determined by electron microscopy (Fig. 5*H*) did not differ between muscles from chow-fed control and CEPT1-MKO mice.

CEPT1 in Human Skeletal Muscle

To determine whether skeletal muscle CEPT1 is related to lipid metabolism and insulin resistance in humans, we studied CEPT1 in skeletal muscle biopsies from two human cohorts. In the first cohort, muscle was obtained from 16 subjects before and after ~20% weight loss, induced by Roux-en-Y gastric bypass or laparoscopic adjustable gastric banding. This intervention decreased adiposity and insulin resistance (Table 2). Skeletal muscle CEPT1 protein

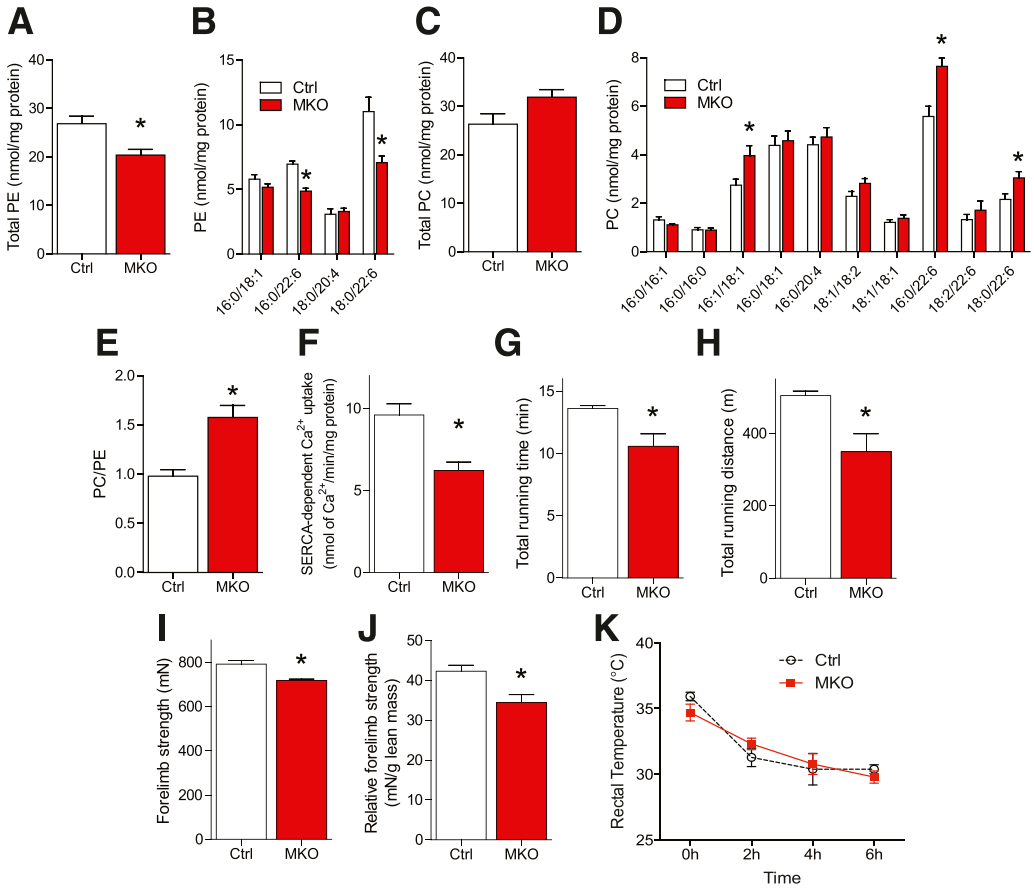

Figure 4—HFD-fed CEPT1-MKO mice have increased SR PC-to-PE ratio, decreased SERCA activity, and decreased muscle contractile function. *A–E*: SR phospholipid composition from gastrocnemius muscles. n = 4/experimental group. *A*: Total SR PE. *B*: Individual SR PE species. *C*: Total SR PC. *D*: Individual SR PC species. *E*: SR PC-to-PE ratio. *F*: SERCA-dependent calcium uptake in gastrocnemius muscles. n = 8/experimental group. *G* and *H*: High-intensity graded exercise treadmill testing. n = 6/experimental group. *G*: Total running time. *H*: Total running distance. *I–J*: Forelimb grip strength test. n = 5–7/experimental group. *I*: Absolute forelimb strength. *J*: Relative forelimb strength. *K*: Cold tolerance test. n = 5/experimental group. Data are means ± SEM. *P < 0.05. Ctrl, control.

abundance was decreased after surgery-induced weight loss (Fig. 6*A* with blots from two representative subjects shown above the graph), suggesting that muscle CEPT1 expression is increased in the human obese state, a finding that parallels the increase in CEPT1 expression seen in mice with HFD feeding (Fig. 2*C* and *D*). Moreover, surgery-induced changes in muscle CEPT1 protein abundance were correlated with surgery-induced changes in glucose R_d (Fig. 6*B*) but not with surgery-induced changes in fat mass (Fig. 6*C*). In the second human cohort, muscle biopsies were obtained from obese subjects (Table 3) representing a range in skeletal muscle insulin sensitivity as assessed by glucose R_d during a hyperinsulinemic-euglycemic clamp procedure. Skeletal muscle CEPT1 mRNA levels were inversely correlated with glucose R_d (Fig. 6*D*), suggesting that lower levels of muscle CEPT1 are associated with improved insulin sensitivity in the setting of human obesity, a finding that parallels the improved insulin sensitivity seen in muscle CEPT1-deficient mice fed an HFD (Fig. 3*F*, *I*, and *K*).

DISCUSSION

How excess lipids interact with muscle to affect glucose metabolism is poorly understood. Caloric excess and physical inactivity promote hyperlipidemia and lipid deposition in skeletal muscle (29), leading to increased lipid content that is associated with insulin resistance (30). However, insulin-sensitive trained athletes also have lipid-laden muscles (18,31), an observation difficult to reconcile with findings in insulin-resistant muscle despite elegant studies of DAGs (32), acylated molecules (33–35), and ceramides (36). To provide novel insights into the complex relationship between lipid excess and insulin sensitivity, we tested the hypothesis that skeletal muscle phospholipid metabolism regulates glucose metabolism.

Our results show that lipid overload in the form of high-fat feeding to mice and obesity in humans is associated with increased expression of CEPT1. HFD induction of CEPT1 in mice increased phospholipid content of skeletal muscle, and disruption of CEPT1 in either cells or mice resulted in phospholipid compositional changes linked to

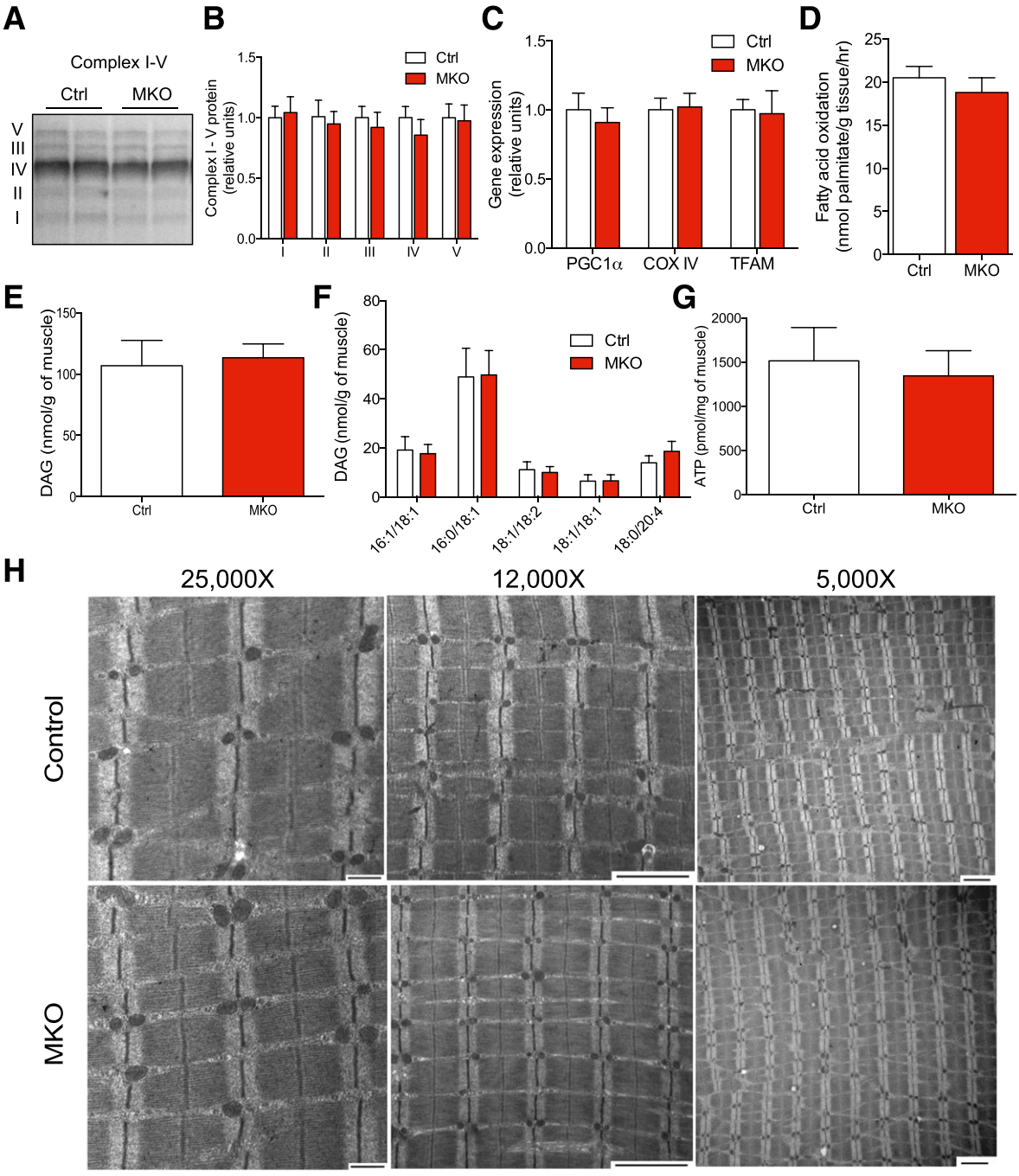

Figure 5—Muscle CEPT1 deficiency in mice does not affect mitochondrial phenotypes or DAG content. *A–D*: Measurements in muscles from HFD-fed mice. *n* = 6/experimental group. *A* and *B*: Western blot quantification of mitochondrial complex I-V in gastrocnemius muscles. *C*: Expression of genes involved in mitochondrial biogenesis in gastrocnemius muscles. *D*: Rates of fatty acid oxidation in gastrocnemius muscles. *E* and *F*: DAG content in soleus muscle of chow-fed mice. *n* = 7/experimental group. *E*: Total DAG content. *F*: DAG species. *G*: ATP content in EDL muscles of chow-fed mice. *n* = 4/experimental group. *H*: Representative electron microscope images at varying magnification from EDL muscles of chow-fed mice. Three animals for each genotype were examined for these studies. Bars in micrographs indicate 500 nm for ×25,000 and 2 μm for ×12,000 and ×5,000. Data are means ± SEM. None of the comparisons were statistically significant. Ctrl, control; hr, hour.

decreased activity of SERCA, which sequesters calcium in the SR to preserve muscle strength. HFD-fed mice with skeletal muscle–specific CEPT1 deficiency had increased insulin sensitivity due to increased glucose transport into muscle. The muscle-specific CEPT1-deficient animals were weak, consistent with decreased SERCA activity.

Our findings in mice have potential translational relevance. CEPT1 mRNA levels are inversely correlated

Table 2—Subjects before and after bariatric surgery–induced weight loss (*N* = 16)

	Before	After
Body weight (kg)	132.9 (117.7–148.1)	107.4 (95.1–119.7)*
BMI (kg/m^2)	46.4 (42.3–50.5)	37.5 (34.2–40.7)*
Body fat (%)	51.3 (48.7–53.8)	46.3 (43.4–49.2)*
Intrahepatic triglyceride content (%)	12.2 (8.2–16.3)	3.9 (2.1–5.8)*
Fasting blood glucose (mg/dL)	95.3 (90.9–99.7)	86.3 (83.3–89.4)*
Fasting blood insulin (μU/mL)	23.9 (20.2–27.7)	9.1 (7.7–10.6)*
Glucose R_d (μmol/min/kg FFM)		
Basal	16.4 (15.3–17.5)	15.2 (14.1–16.3)
Clamp	36.7 (30.2–43.1)	57.4 (50.6–64.1)*

Data are means (95% CI). Roux-en-Y gastric bypass, 2 male/5 female subjects; laparoscopic adjustable gastric banding, 1 male/8 female subjects; age 46.0 years (40.2–51.7). FFM, fat-free mass. *$P < 0.05$.

with insulin sensitivity, and weight loss in obese humans decreases skeletal muscle CEPT1 protein. The latter change correlated with insulin sensitivity but not fat mass, suggesting that CEPT1 and its products, as opposed to potentially toxic effects of other lipids, may play a role in human insulin resistance.

These results suggest that lipid excess induces SR phospholipid adaptation in skeletal muscle and implicate CEPT1 as an important enzyme for maintaining SR functional integrity. The SR releases calcium to allow contraction and sequesters calcium through the activity of SERCA to allow relaxation. Our data show that HFD feeding increases SR phospholipid abundance, mediated in part by an induction of CEPT1 that preserves the PC-to-PE ratio, a known determinant of SERCA activity (7,37). In the absence of muscle CEPT1, an increased PC-to-PE ratio decreases SERCA activity, causing muscle weakness (26).

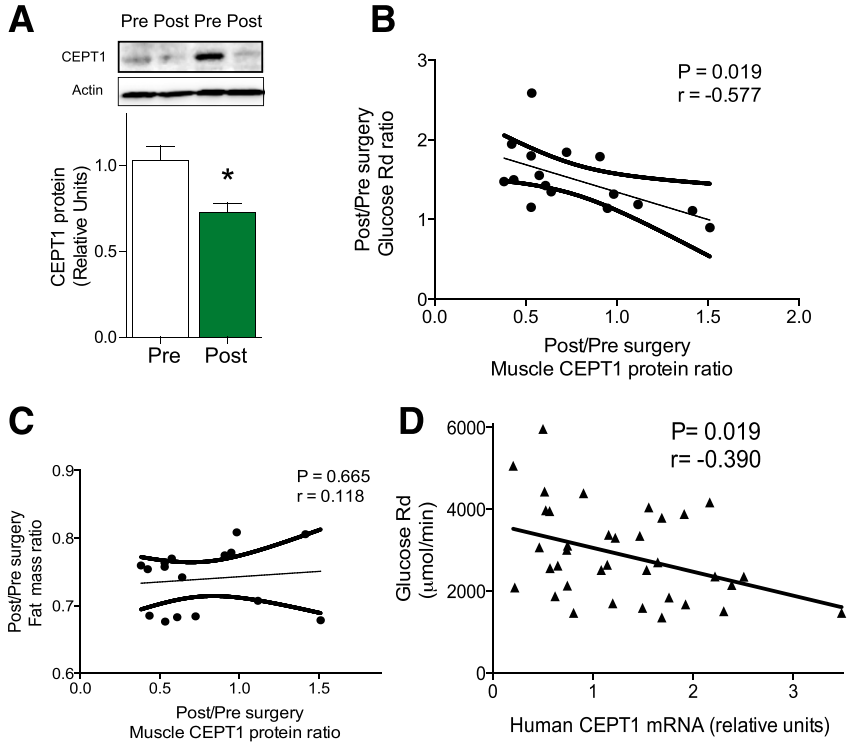

Figure 6—Human muscle CEPT1 is associated with obesity-induced insulin resistance. *A–C*: Human muscle CEPT1 protein abundance in 16 subjects (see Table 2 for characteristics) pre–gastric bypass surgery (pre) and post–gastric bypass surgery (post). *A*: Western blot quantification of muscle CEPT1 protein. Data are means ± SEM. *$P < 0.05$. *B*: Pearson correlation analysis between changes in muscle CEPT1 protein abundance and changes in glucose disposal rate. *C*: Pearson correlation analysis between changes in muscle CEPT1 protein abundance and changes in fat mass. *D*: Pearson correlation analysis of human muscle CEPT1 mRNA expression and glucose disposal rate determined by clamp for 39 obese subjects of varying metabolic health. (See Table 3 for characteristics.)

Table 3—Obese subjects with varying metabolic health (*N* = 39)

n (male/female)	6/33
Age (years)	40.2 (36.6–43.8)
Body weight (kg)	95.3 (87.3–103.2)
BMI (kg/m^2)	33.5 (30.9–36.1)
Body fat (%)	43.4 (40.6–46.3)
Visceral adipose tissue (cm^3)	1,341.6 (1,087.1–1,596.2)
Intrahepatic triglyceride content (%)	8.45 (5.39–11.51)
Fasting blood glucose (mg/dL)	93.0 (90.9–95.2)
Fasting blood insulin (μU/mL)	15.36 (12.47–18.26)
HOMA-IR	3.57 (2.87–4.26)
Fasting blood free fatty acids (μmol/L)	0.56 (0.52–0.61)

Data are means (95% CI). HOMA-IR, HOMA of insulin resistance.

Both CEPT1 and FAS increase in muscle with high-fat feeding. Muscle CEPT1 deficiency appears to mirror muscle FAS deficiency (5). Both models have a normal phenotype on a chow diet, and both develop the same degree of adiposity as littermate controls with high-fat feeding. Diet-induced obesity in mice with deficiency of CEPT1 or FAS in muscle resulted in increased insulin sensitivity. The latter is likely caused by altered calcium flux. Increased cystosolic calcium signaling, seen with both CEPT1 and FAS deficiency, is a known muscle insulin sensitizer (9,38–41). One interpretation of the similarities between the FAS-deficient and CEPT1-deficient phenotypes in muscle is that FAS and CEPT1 coordinately channel lipids to compartments responsible for maintaining contractile function in the setting of high-fat feeding. HFDs compromise exercise performance (42–44), suggesting that FAS-CEPT1 lipid channeling may compensate for detrimental dietary effects on muscle function. Lipid compartmentalization in muscle is known to occur with acyl-CoA molecules (45).

Muscle FAS deficiency and CEPT1 deficiency are independently characterized by selective decreases in SR PE content only in the setting of high-fat feeding, consistent with the notion that FAS and CEPT1 coordinately channel lipids, since either deficiency impacts the same class of lipids at the same site. Since PE increases the affinity of calcium for SERCA in lipid bilayers (8), decreasing its content in the setting of CEPT1 or FAS deficiency provides a molecular explanation underlying impaired SERCA activity with an altered PC-to-PE ratio. Increasing SERCA1 expression restores SERCA enzyme activity and eliminates AMP activation caused by FAS deficiency (5), suggesting that SERCA activity is more important than the PC-to-PE ratio for insulin action. Neither FAS nor CEPT1 deficiency appears to impact mitochondrial function, which might be predicted based on previous data suggesting that mitochondrial PE is generated on the mitochondrial inner membrane through the action of phosphatidylserine decarboxylase (46,47).

While this work was in preparation, ECT-deficient mice were described (28). Like FAS and CEPT1 deficiency with low-fat feeding, these animals have no insulin sensitivity phenotype on a chow diet. Unlike the FAS and CEPT1 models, these mice have a mitochondrial phenotype, perhaps due to forced reliance on the activity of phosphatidylserine decarboxylase to generate the PE detected in these animals. Other features complicate comparisons between the different models. The ECT-deficient mouse was generated using the muscle creatine kinase Cre, expressed in adult heart (48), suggesting that altered myocardial function could impact skeletal muscle metabolism through altered perfusion. FAS- and CEPT1-deficient mice were generated using HSA-Cre, which is not expressed in adult heart (5). Lipid channeling involving FAS and CEPT1 is likely because FAS is substantially associated with SR in muscle (5) and CEPT1 is predominantly an SR/ER enzyme. ECT, unlike the choline-specific enzyme directly upstream of CEPT1 in the Kennedy pathway, appears to be predominantly cytosolic (49), suggesting that only a subfraction of this enzyme at the SR would be required for directed lipid synthesis.

In summary, the loss of muscle CEPT1 in mice increases insulin sensitivity but impairs muscle strength in the setting of an HFD. In obese humans, weight loss decreases CEPT1 protein, and these changes are correlated with insulin sensitivity but not fat mass. In a separate group of humans, skeletal muscle CEPT1 mRNA was inversely associated with insulin sensitivity. The phenotypes of skeletal muscle–specific CEPT1 deficiency and skeletal muscle–specific FAS deficiency appear to be the same, suggesting that these lipogenic proteins participate in the channeling of lipids to PE pools at the SR. The coordinate induction of FAS and CEPT1 in muscle in the setting of insulin resistance may be required to maintain muscle functional integrity. Identifying specific PE species linked to muscle function in humans could lead to novel therapies for sustaining muscle contraction in the obese, a strategy that could promote health.

Funding. This work was funded by National Institute of Diabetes and Digestive and Kidney Diseases, National Institutes of Health, grants DK-101392, DK-076729, DK-020579, DK-056341, DK-094874, DK-095505, and DK-095774 (the last two to K.F.).

Duality of Interest. No potential conflicts of interest relevant to this article were reported.

Author Contributions. K.F. designed experiments, contributed to all data unless otherwise noted, and wrote the manuscript. I.J.L. conceived the experiment and generated floxed CEPT1 mice. L.D.S. assayed DAG and ATP in muscle, processed samples for electron microscopy, and performed hyperinsulinemic-euglycemic clamp studies. L.Y. performed hyperinsulinemic-euglycemic clamp studies. H.S. conducted phospholipidomic analyses. S.K. contributed to study design, generated data involving humans, and revised the manuscript. C.F.S. designed experiments and wrote the manuscript. K.F. is the guarantor of this work and, as such, had full access to all the data in the study and takes responsibility for the integrity of the data and the accuracy of the data analysis.

Prior Presentation. Parts of this study were presented in abstract form at the 74th Scientific Sessions of the American Diabetes Association, San Francisco, CA, 13–17 June 2014.

References

1. Booth FW, Gordon SE, Carlson CJ, Hamilton MT. Waging war on modern chronic diseases: primary prevention through exercise biology. J Appl Physiol (1985) 2000;88:774–787
2. Hawley JA, Hargreaves M, Joyner MJ, Zierath JR. Integrative biology of exercise. Cell 2014;159:738–749
3. Schenk S, Saberi M, Olefsky JM. Insulin sensitivity: modulation by nutrients and inflammation. J Clin Invest 2008;118:2992–3002
4. DeFronzo RA, Gunnarsson R, Björkman O, Olsson M, Wahren J. Effects of insulin on peripheral and splanchnic glucose metabolism in noninsulin-dependent (type II) diabetes mellitus. J Clin Invest 1985;76:149–155
5. Funai K, Song H, Yin L, et al. Muscle lipogenesis balances insulin sensitivity and strength through calcium signaling. J Clin Invest 2013;123: 1229–1240
6. Kersten S. Mechanisms of nutritional and hormonal regulation of lipogenesis. EMBO Rep 2001;2:282–286
7. Fu S, Yang L, Li P, et al. Aberrant lipid metabolism disrupts calcium homeostasis causing liver endoplasmic reticulum stress in obesity. Nature 2011; 473:528–531
8. Gustavsson M, Traaseth NJ, Veglia G. Activating and deactivating roles of lipid bilayers on the Ca(2+)-ATPase/phospholamban complex. Biochemistry 2011;50:10367–10374
9. Wright DC, Hucker KA, Holloszy JO, Han DH. Ca2+ and AMPK both mediate stimulation of glucose transport by muscle contractions. Diabetes 2004;53:330–335
10. Goonasekera SA, Lam CK, Millay DP, et al. Mitigation of muscular dystrophy in mice by SERCA overexpression in skeletal muscle. J Clin Invest 2011;121: 1044–1052
11. Gehrig SM, van der Poel C, Sayer TA, et al. Hsp72 preserves muscle function and slows progression of severe muscular dystrophy. Nature 2012;484: 394–398
12. Henneberry AL, Wright MM, McMaster CR. The major sites of cellular phospholipid synthesis and molecular determinants of Fatty Acid and lipid head group specificity. Mol Biol Cell 2002;13:3148–3161
13. Miniou P, Tiziano D, Frugier T, Roblot N, Le Meur M, Melki J. Gene targeting restricted to mouse striated muscle lineage. Nucleic Acids Res 1999; 27:e27
14. Gan Z, Burkart-Hartman EM, Han DH, et al. The nuclear receptor PPARβ/δ programs muscle glucose metabolism in cooperation with AMPK and MEF2. Genes Dev 2011;25:2619–2630
15. Funai K, Cartee GD. Inhibition of contraction-stimulated AMP-activated protein kinase inhibits contraction-stimulated increases in PAS-TBC1D1 and glucose transport without altering PAS-AS160 in rat skeletal muscle. Diabetes 2009;58:1096–1104
16. Moore L, Chen T, Knapp HR Jr, Landon EJ. Energy-dependent calcium sequestration activity in rat liver microsomes. J Biol Chem 1975;250:4562–4568
17. Lodhi IJ, Yin L, Jensen-Urstad AP, et al. Inhibiting adipose tissue lipogenesis reprograms thermogenesis and PPARγ activation to decrease diet-induced obesity. Cell Metab 2012;16:189–201
18. Amati F, Dubé JJ, Alvarez-Carnero E, et al. Skeletal muscle triglycerides, diacylglycerols, and ceramides in insulin resistance: another paradox in endurance-trained athletes? Diabetes 2011;60:2588–2597
19. Magkos F, Bradley D, Schweitzer GG, et al. Effect of Roux-en-Y gastric bypass and laparoscopic adjustable gastric banding on branched-chain amino acid metabolism. Diabetes 2013;62:2757–2761
20. Fabbrini E, Magkos F, Mohammed BS, et al. Intrahepatic fat, not visceral fat, is linked with metabolic complications of obesity. Proc Natl Acad Sci U S A 2009; 106:15430–15435
21. Korenblat KM, Fabbrini E, Mohammed BS, Klein S. Liver, muscle, and adipose tissue insulin action is directly related to intrahepatic triglyceride content in obese subjects. Gastroenterology 2008;134:1369–1375
22. English AR, Voeltz GK. Rab10 GTPase regulates ER dynamics and morphology. Nat Cell Biol 2013;15:169–178
23. Kraegen EW, James DE, Storlien LH, Burleigh KM, Chisholm DJ. In vivo insulin resistance in individual peripheral tissues of the high fat fed rat: assessment by euglycaemic clamp plus deoxyglucose administration. Diabetologia 1986;29:192–198
24. Albers PH, Pedersen AJ, Birk JB, et al. Human muscle fiber type-specific insulin signaling: impact of obesity and type 2 diabetes. Diabetes 2015;64: 485–497
25. Turner N, Lee JS, Bruce CR, et al. Greater effect of diet than exercise training on the fatty acid profile of rat skeletal muscle. J Appl Physiol (1985) 2004;96:974–980
26. Berchtold MW, Brinkmeier H, Müntener M. Calcium ion in skeletal muscle: its crucial role for muscle function, plasticity, and disease. Physiol Rev 2000;80: 1215–1265
27. Bal NC, Maurya SK, Sopariwala DH, et al. Sarcolipin is a newly identified regulator of muscle-based thermogenesis in mammals. Nat Med 2012;18: 1575–1579
28. Selathurai A, Kowalski GM, Burch ML, et al. The CDP-ethanolamine pathway regulates skeletal muscle diacylglycerol content and mitochondrial biogenesis without altering insulin sensitivity. Cell Metab 2015;21: 718–730
29. Funai K, Semenkovich CF. Skeletal muscle lipid flux: running water carries no poison. Am J Physiol Endocrinol Metab 2011;301:E245–E251
30. Pan DA, Lillioja S, Kriketos AD, et al. Skeletal muscle triglyceride levels are inversely related to insulin action. Diabetes 1997;46:983–988
31. Goodpaster BH, He J, Watkins S, Kelley DE. Skeletal muscle lipid content and insulin resistance: evidence for a paradox in endurance-trained athletes. J Clin Endocrinol Metab 2001;86:5755–5761
32. Samuel VT, Shulman GI. Mechanisms for insulin resistance: common threads and missing links. Cell 2012;148:852–871
33. Li LO, Klett EL, Coleman RA: Acyl-CoA synthesis, lipid metabolism and lipotoxicity. Biochim Biophys Acta 2010;1801:246–251
34. Muoio DM, Neufer PD. Lipid-induced mitochondrial stress and insulin action in muscle. Cell Metab 2012;15:595–605
35. Schooneman MG, Vaz FM, Houten SM, Soeters MR. Acylcarnitines: reflecting or inflicting insulin resistance? Diabetes 2013;62:1–8
36. Chavez JA, Summers SA. A ceramide-centric view of insulin resistance. Cell Metab 2012;15:585–594
37. Fu S, Watkins SM, Hotamisligil GS. The role of endoplasmic reticulum in hepatic lipid homeostasis and stress signaling. Cell Metab 2012;15: 623–634
38. Witczak CA, Fujii N, Hirshman MF, Goodyear LJ. Ca2+/calmodulin-dependent protein kinase kinase-alpha regulates skeletal muscle glucose uptake independent of AMP-activated protein kinase and Akt activation. Diabetes 2007; 56:1403–1409
39. Xie X, Gong Z, Mansuy-Aubert V, et al. C2 domain-containing phosphoprotein CDP138 regulates GLUT4 insertion into the plasma membrane. Cell Metab 2011;14:378–389
40. Kramer HF, Taylor EB, Witczak CA, Fujii N, Hirshman MF, Goodyear LJ. Calmodulin-binding domain of AS160 regulates contraction- but not insulin-stimulated glucose uptake in skeletal muscle. Diabetes 2007;56:2854–2862
41. Park DR, Park KH, Kim BJ, Yoon CS, Kim UH. Exercise ameliorates insulin resistance via Ca2+ signals distinct from those of insulin for GLUT4 translocation in skeletal muscles. Diabetes 2015;64:1224–1234
42. Starling RD, Trappe TA, Parcell AC, Kerr CG, Fink WJ, Costill DL. Effects of diet on muscle triglyceride and endurance performance. J Appl Physiol (1985) 1997;82:1185–1189

43. Fleming J, Sharman MJ, Avery NG, et al. Endurance capacity and high-intensity exercise performance responses to a high fat diet. Int J Sport Nutr Exerc Metab 2003;13:466–478
44. Erlenbusch M, Haub M, Munoz K, MacConnie S, Stillwell B. Effect of high-fat or high-carbohydrate diets on endurance exercise: a meta-analysis. Int J Sport Nutr Exerc Metab 2005;15:1–14
45. Li LO, Grevengoed TJ, Paul DS, et al. Compartmentalized acyl-CoA metabolism in skeletal muscle regulates systemic glucose homeostasis. Diabetes 2015;64:23–35
46. Zborowski J, Dygas A, Wojtczak L. Phosphatidylserine decarboxylase is located on the external side of the inner mitochondrial membrane. FEBS Lett 1983;157:179–182
47. van der Veen JN, Lingrell S, da Silva RP, Jacobs RL, Vance DE. The concentration of phosphatidylethanolamine in mitochondria can modulate ATP production and glucose metabolism in mice. Diabetes 2014;63:2620–2630
48. Laustsen PG, Russell SJ, Cui L, et al. Essential role of insulin and insulin-like growth factor 1 receptor signaling in cardiac development and function. Mol Cell Biol 2007;27:1649–1664
49. Vermeulen PS, Tijburg LB, Geelen MJ, van Golde LM. Immunological characterization, lipid dependence, and subcellular localization of CTP:phosphoethanolamine cytidylyltransferase purified from rat liver. Comparison with CTP:phosphocholine cytidylyltransferase. J Biol Chem 1993;268:7458–7464